AD-A103 063 MASSACHUSETTS INST OF TECH LEXINGTON LINCOLN LAB F/G 17/7
PRECISION STANDOFF GUIDANCE ANTENNA ACCURACY EVALUATION,(U)
FEB 81 F H IRONS, M M LANDESBERG F19628-80-C-0002
UNCLASSIFIED TR-543 ESD-TR-81-6 NL

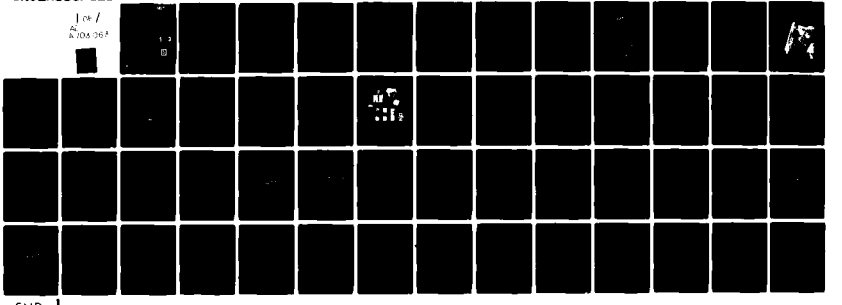

END
DATE FILMED
9-81
DTIC

Technical Report

543

Precision Standoff Guidance Antenna Accuracy Evaluation

F. H. Irons
M. M. Landesberg

18 February 1981

Prepared for the Department of the Air Force
under Electronic Systems Division Contract F19628-80-C-0002 by

Lincoln Laboratory
MASSACHUSETTS INSTITUTE OF TECHNOLOGY
LEXINGTON, MASSACHUSETTS

The work reported in this document was performed at Lincoln Laboratory, a center for research operated by Massachusetts Institute of Technology, with the support of the Department of the Air Force under Contract F19628-80-C-0002.

The views and conclusions contained in this document are those of the contractor and should not be interpreted as necessarily representing the official policies, either expressed or implied, of the United States Government.

This technical report has been reviewed and is approved for publication.

FOR THE COMMANDER

Raymond L. Loiselle, Lt. Col., USAF
Chief, ESD Lincoln Laboratory Project Office

MASSACHUSETTS INSTITUTE OF TECHNOLOGY

LINCOLN LABORATORY

PRECISION STANDOFF GUIDANCE ANTENNA ACCURACY EVALUATION

F.H. IRONS

Group 44

M.M. LANDESBERG

GTE Products

TECHNICAL REPORT 543

18 FEBRUARY 1981

LEXINGTON MASSACHUSETTS

ABSTRACT

This report presents a summary of work done to determine the inherent angular accuracy achievable with the guidance and control precision standoff guidance antenna. The antenna is a critical element in the anti-jam single station guidance program since its characteristics can limit the intrinsic location guidance accuracy. It was important to determine the extent to which high ratio beamsplitting results could be achieved repeatedly and what issues were involved with calibrating the antenna.

The antenna accuracy has been found to be on the order of 0.006° through the use of a straightforward lookup table concept. This corresponds to a cross range error of 21 m at a range of 200 km. This figure includes both pointing errors and off-axis estimation errors.

It was found that the antenna off-boresight calibration is adequately represented by a straight line for each position plus a lookup table for pointing errors relative to broadside. In the event recalibration is required, it was found that only 1% of the model would need to be corrected.

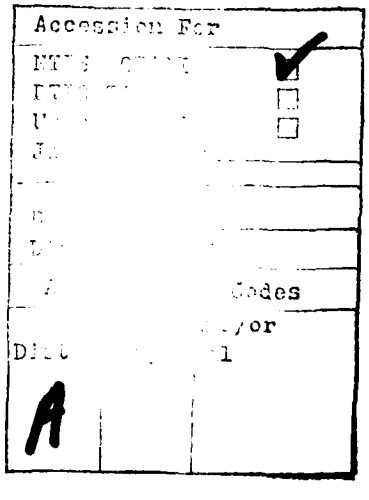

CONTENTS

LIST OF ILLUSTRATIONS

LIST OF ILLUSTRATIONS (continued)

LIST OF TABLES

PRECISION STANDOFF GUIDANCE ANTENNA ACCURACY EVALUATION

I. INTRODUCTION

The overall program addresses the problem of single station precision standoff guidance of weapon platforms and sensors in a tactical environment. The operational concept is shown in Fig. 1 where the single station guidance platform is located well behind the FEBA and is required to guide a variety of platforms to specified target locations protected by jammers. The guidance platform will utilize a phased array antenna to provide guidance of multiple remote terminals.

The accuracy of direction-of-arrival (DOA) estimation is the fundamental problem in developing single station standoff guidance. The necessary angular accuracy to place a remote terminal within a 50 m cross range tolerance is 0.0143 degrees. A candidate cross range error budget for the system is shown in Table 1, which indicates that the Precision Standoff Guidance Antenna (PSGA) should support accuracies of the order of 0.008 degrees. This includes both a boresight pointing error and a beam splitting error.

This report establishes the measured direction of arrival accuracy obtained with the Precision Standoff Guidance Antenna (PSGA) using ground-to-ground CW measurements. Sections 2 and 3 present the antenna characteristics and the methodology of DOA estimation. Section 4 discusses the calibration or measurement testbed including the antenna range, hardware description and software capability. Section 5 presents typical beam pointing error and monopulse slope measurements. Sections 6 and 7 discuss the long term performance of the array and the effectiveness of our calibration model. Section 8 describes possible temperature compensation terms to be used to further improve the model performance.

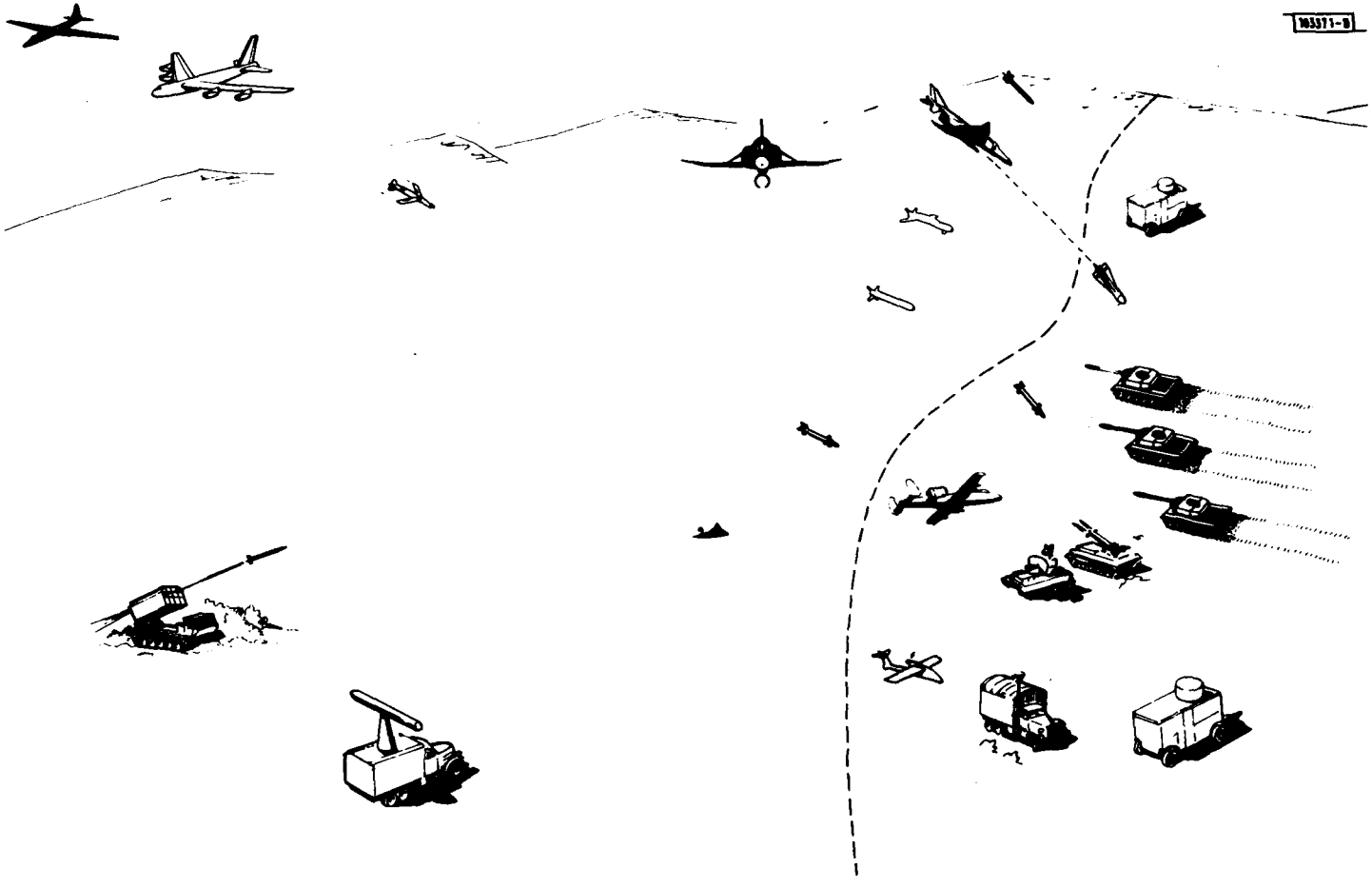

Fig. 1. Single station guidance concept.

TABLE 1

CROSS RANGE ERROR BUDGET REQUIREMENTS

Total allowed rms cross range error at 200 km		0.0143° (50m)
Guidance Platform Location Allowance		
INS Yaw Error	0.009	
Platform Location (10m)	0.003	
Altitude (2° pitch, 10 km difference, 150m uncertainty)	0.004	0.010°
Allowance for Other Errors, e.g., Jamming, Propagation, etc.		0.006°
Required Antenna Calibration Beampointing and Beamsplitting		0.0080° (28m)

II. ANTENNA CHARACTERISTICS

Figure 2 shows the experimental PSGA on the pedestal used for the Lincoln Laboratory D building antenna range. The antenna is a J-band phased array with a vertical H plane horn flare, and is linear horizontally polarized. It is 2.5 meters long, consists of 208 elements, and is installed in a 3 meter cylindrical pod.

Each element utilizes a 3-bit pin diode microstrip phase shifter which has input and output dipole radiators. Energy is coupled from a waveguide feed to the input dipole and propagated via the output dipole through the antenna aperture. Azimuth scanning is controlled via a beam steering computer programmer. The array consists of sixteen (16) identical subarrays. Each subarray is comprised of a broad wall to narrow wall directional coupler having 13 secondary arms, with (13) enclosed phase shifters, and an associated antenna flared aperture. Use of the identical subarray concept is possible as the result of the amplitude taper provided by the corporate structure feeding the subarrays. This structure is a 4 level 16 way equal time delay waveguide network. In order to achieve the desired 20 dB sidelobe performance, a piecewise best fit to a 25 dB, $\bar{N} = 5$ Taylor weighting was selected. Predicted amplitude tapers of 8.7 dB and 1.1 dB in the corporate structure and the subarray, respectively, adequately approximate the ideal illumination (in actuality, the subarray taper was 2 dB due to its inherent design). Amplitude-wise, the corporate structure's coupling values are more dominant than the subarray tapers with regard to the effect upon the radiation characteristics. The effect of phase illumination errors upon the antenna pattern is more important than the amplitude illumination variance [1]. Thus, adherence to the sidelobe criteria required that the rms phase error be held to some minimal value. The aperture's phase characteristic is effectively scrambled as the result of a combination of the 90° phase shifts inherent in the corporate structure hybrids, the subarray differential path lengths, and the phase shifter tolerances. These phase disparities, which are useful in altering the quantized phase effects, are accounted for in the collimation process at the time of manufacture [2].

A summary of the key antenna performance parameters is listed in Table 2.

106960-S

Fig. 2. Phased array antenna and receiver box.

TABLE 2

KEY ANTENNA PERFORMANCE PARAMETERS

PHYSICAL	
Type	Phased Scanned Linear Array
Number of Elements	208
Phase Shifters	3-bit Pin Diode
Array Length	2.5m
Polarization	Horizontal
PERFORMANCE	
Operating Frequency Band	16.00-16.50 GHz
Instantaneous Bandwith	30 MHz
Field of View	± 30°
Beamwidth	
Azimuth	0.5°
Elevation	26°
Gain	28 dBi
Sidelobes	< -20 dB
OPERATION	
Number of Beam Positions	961
Step Size	0.0625°
Number of Operating Frequencies	51
Step Size	10 MHz

III. DIRECTION OF ARRIVAL ESTIMATION

The antenna measurement program was designed to assess the antenna capability for supporting a DOA accuracy goal of 0.008°. Figure 3 depicts how the antenna would be used to make a precision angle measurement upon a cooperative remote terminal (e.g., a weapon denoted by the "x").

The remote terminal would be illuminated by a nearby beam, for example, that centered at the angle θ_o. Next a beamsplit discriminant D would be calculated, and the target offset $\Delta\theta(D)$ from the beam center would be deducted from D. The angle θ of the target then would be determined from the expression

$$\theta = \theta_o + \Delta\theta(D) \qquad (1)$$

The initial antenna measurements were designed to explore whether the terms θ_o and $\Delta\theta(D)$ in Eq. (1) could be determined with accuracies that are supportive of the 0.008° accuracy goal for θ.

The accuracy with which the θ_o can be determined is the accuracy to which the beam center is known. If one had total control over the illumination function across the antenna aperture, then the beam center would be known exactly. However, one does not have total control over the illumination function. Specifically, the phases of the radiating elements differ from the ideal phases for the direction θ_o due to a variety of factors that include unequal time delays in the antenna corporate feed, phase-shifter quantizations and non-uniformities among the phase shifters. Accordingly, the actual illumination function equals the ideal function plus a perturbation (or noise) function due to phase errors. The noise illumination function is added to the ideal function and the total produces the actual far field radiation pattern. Due to the noise far field the actual beam center typically is shifted from the desired beam center, producing a beam pointing error. It is this error that prevents the term θ_o in Eq. (1) from being known exactly.

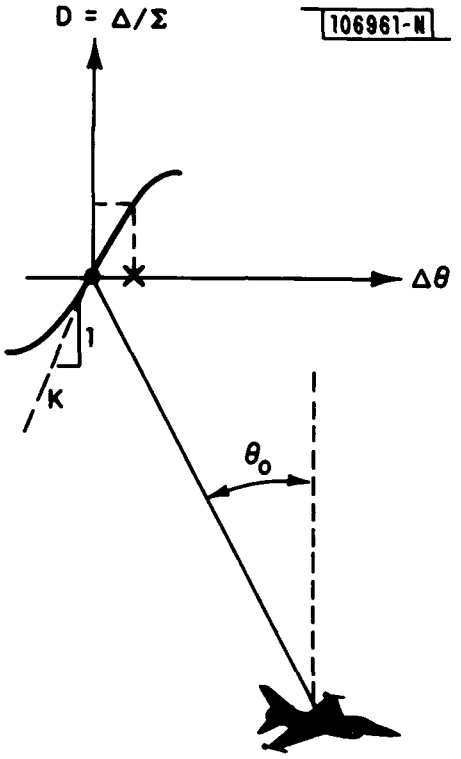

Fig. 3. Direction of arrival estimation.

The ϑ_o uncertainty is composed of two parts, namely a time invariant part and a time variant part. The goal of the calibration will be to eliminate most of the time invariant error. The residual error is required to be less than the 0.008° goal.

The accuracy with which the target offset $\Delta\theta$ can be determined is the accuracy to which the monopulse discrimination function is known and modeled. The monopulse discriminant is derived by a ratio of the received signals from the sum and difference antenna patterns. Thus, the monopulse function is dependent upon the relative shape of the antenna pattern main lobes and the gain of the receiving channel. We have hypothesized a linear monopulse function discriminant $\Delta\theta(D) = K\,D$ and shall evaluate the residual error affecting target position estimation.

The true angle θ to the target is

$$\theta = \theta_c + \vartheta_\varepsilon + K(\Delta/\Sigma) + \vartheta_r \qquad (2)$$

where

θ_c is the commanded beam position
ϑ_ε is the error in the beam pointing position
(Δ/Σ) is the measured monopulse signal
K is the monopulse discrimination function.
θ_r is the residual error of the monopulse measurement

IV. CALIBRATION SYSTEM

The angular accuracy obtainable with this system is a direct measure of the stability of ϑ_ε and K. Obtaining a time history of these parameters is an enormous task. As a result, a fully automatic measurement and assessment program was developed consisting of a hardware test bed and computer programs for data acquisition and evaluation.

A hardware testbed was assembled, as shown in Figs. 4 and 5, to assess the antenna performance and to provide automated calibration of the system. Figure 4 shows the testbed in schematic form whereas Fig. 5 shows it pictorally. The components of this system include the antenna, the beamsplit processor for CW signals, and a source transmitter, all under computer control. Two transmitters were used for the experiment. A fixed frequency of 16.4 GHz was mounted on the Billerica Water Tower 9.6 km away, and a remotely programmable source was mounted on the DABS tower 0.5 km away. The programmable source was controlled via a telephone modem link and covered the frequency range from 16.00 to 16.50 GHz in 10 MHz steps. Both transmitters were operated in a CW transmit mode.

A topographical map showing the relative locations of the receiving pedestal and the two transmitters is shown in Fig. 6.

The phased array, operated as a receiver, was mounted on a Scientific Atlanta pedestal which was rotated under computer control to make pattern measurements for a predetermined set of measurement parameters. Azimuth angles are measured using a 19-bit shaft encoder and the patterns are sampled with 12-bit A/D converters on the I and Q baseband signals for both the Σ and Δ signals.

The calibration program consists of four routines. The first verified the alignment of the down converter parameters by measuring the relative gain, quadrature phase, and DC offset of the sum and difference I and Q channels. The second is used to control the antenna pattern measurement parameters. Inputs to this consist of the following:

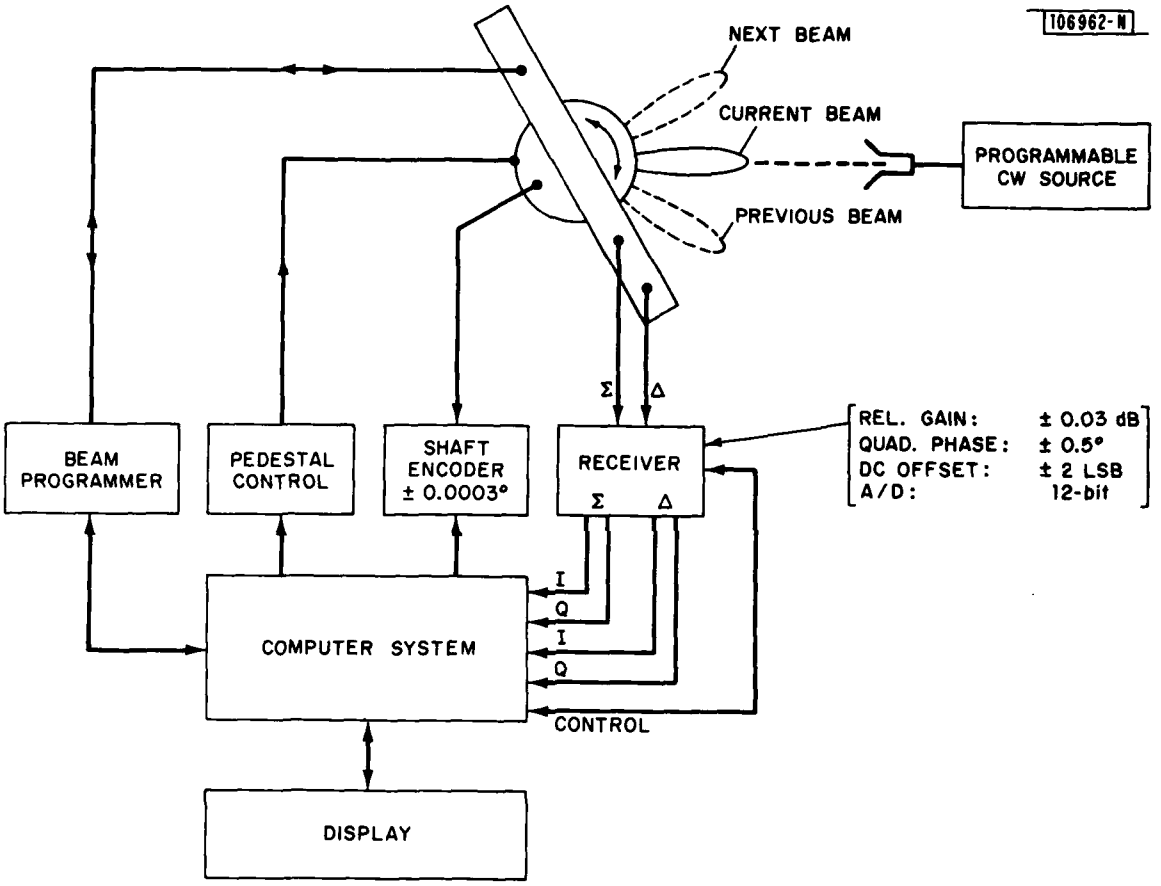

Fig. 4. Automated antenna calibration system.

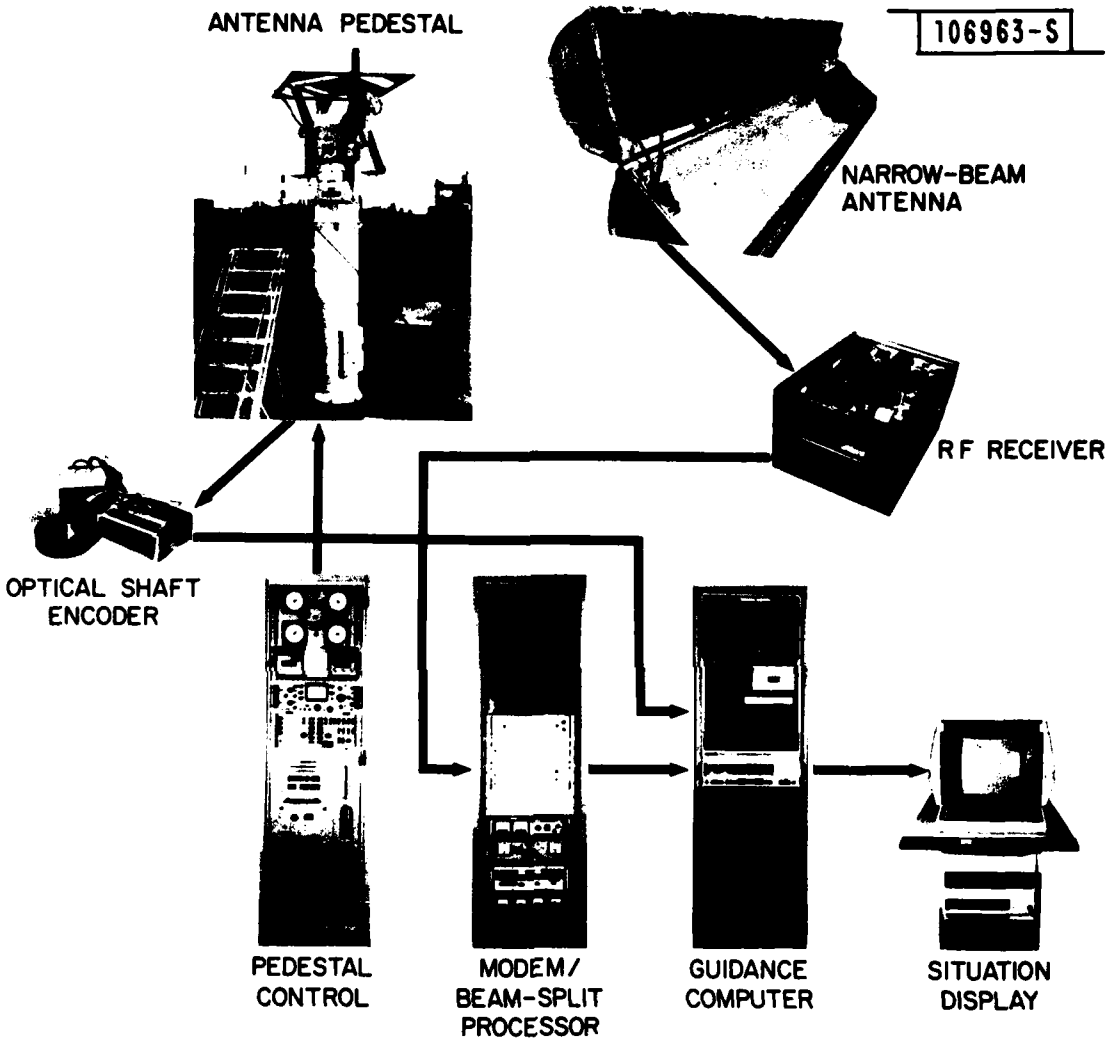

Fig. 5. Components of CW calibration system.

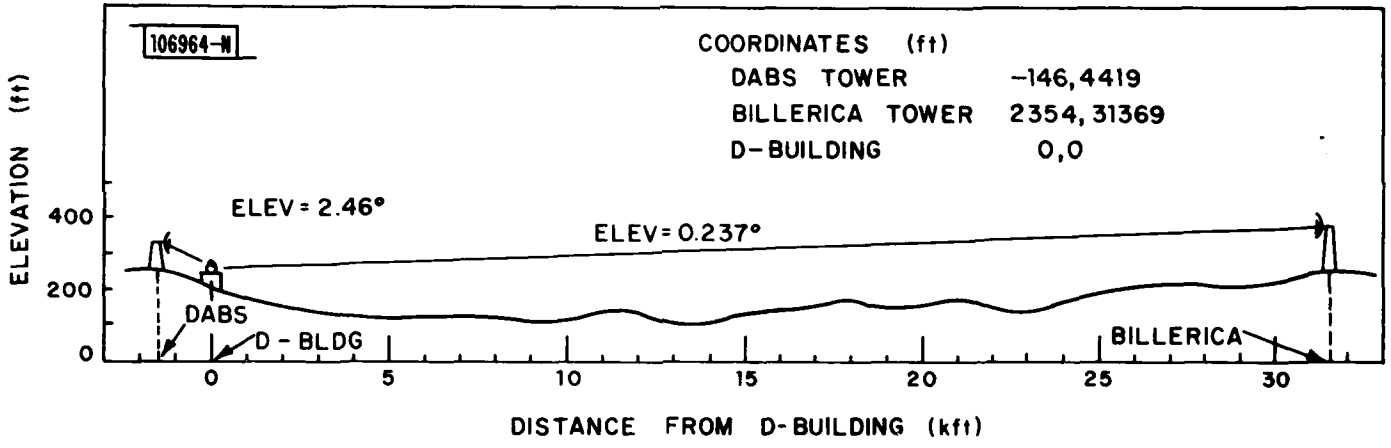

Fig. 6. Topography of PSGA test range.

1. a set of 1 to n antenna beam positions.
2. measurement frequency
3. measurement angular interval
4. pedestal rotation rate
5. A/D sample rate
6. Downconverter parameters

The third routine provides the real-time control of the antenna beam programmer and the pedestal while also collecting and storing the shaft encoder and digitized sum and difference received signals. This system was capable of collecting about six patterns per minute. A pattern generally consisted of about 100 points spanning two degrees in azimuth. The data were all stored on hard disks for editing by the fourth routine.

The edit routine can retrieve, analyze and plot about six patterns per minute. The edit program is designed to provide rapid assessment of the antenna beampointing performance which is measured in terms of the beampointing error and the monopulse discrimination function.

As an optional first step, plots of the sum and difference antenna patterns for any measured beam position are provided. A typical measured pattern pair is shown in Fig. 7. The patterns are plotted over a 1° interval and are well behaved and symmetrical. The number of frequency-beam position combinations precludes examination of all possible individual patterns to determine the beam pointing accuracy assessment or calibration.

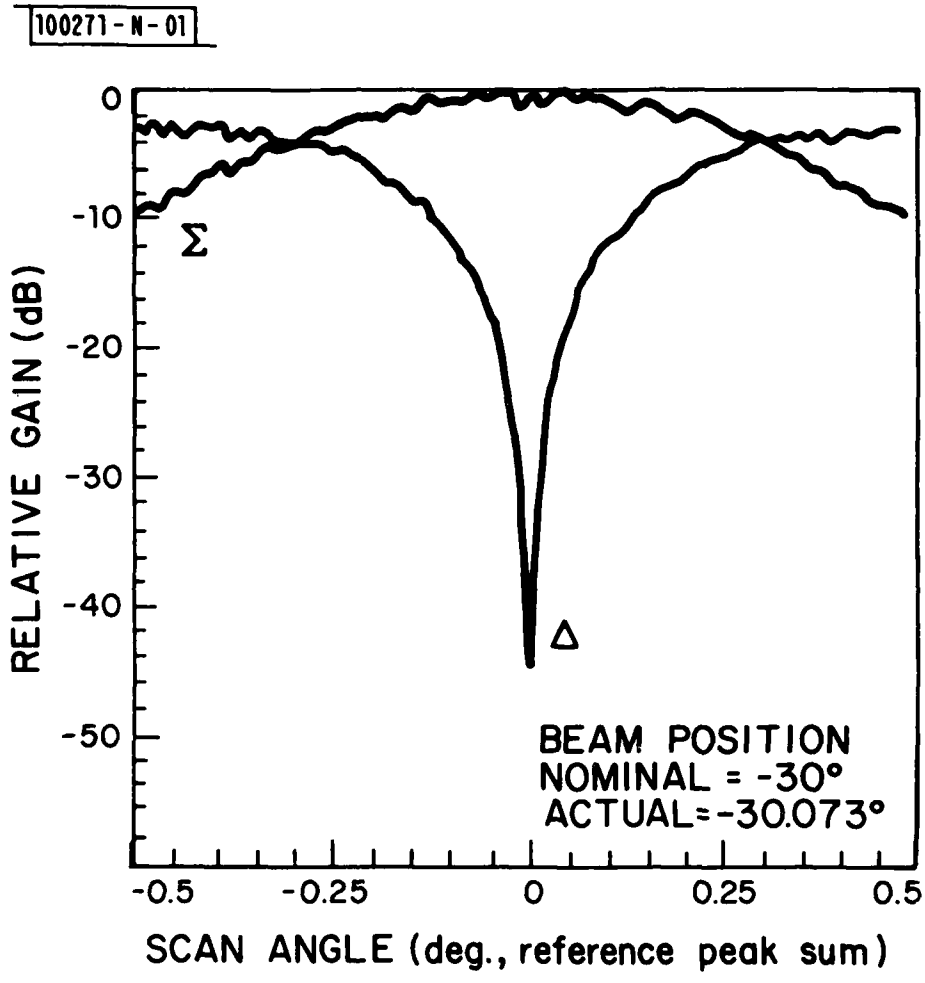

Fig. 7. Typical pattern measurement.

V. BEAMPOINTING MEASUREMENT RESULTS

For the antenna metric accuracy evaluation, each antenna pattern pair must be automatically reduced to an estimate of beam pointing position and monopulse slope. Ultimately, the beam pointing position is defined as the zero crossing of the monopulse discrimination function. To obtain an unbiased estimate, a measured data interval symmetrically centered about the actual beam pointing position must be used. This implies an iterative approach of estimating beam pointing position and then using this estimate to refine the data base. To avoid this iterative approach, an estimate of beam pointing position which is less susceptible to errors in the initial guess must be used. The selected computer algorithm finds a sum pattern peak near the commanded beam pointing position and performs a quadratic least squares estimate to the main lobe using the data within ±0.25 degrees of the commanded beam position.

The quadratic function estimate of the beam center is used to select the data interval for determining the monopulse discrimination function (MPF). Each data point within ±0.15 degrees of this boresight reference is processed using the following formulation:

$$MPF = \frac{\Delta}{\Sigma} \cos\left(\varphi_{\Delta} - \varphi_{\Sigma} - \varphi_{B}\right) \qquad (3)$$

where

- Δ is difference signal amplitude
- Σ is sum signal amplitude
- ϕ_{Δ} is difference signal phase
- ϕ_{Σ} is sum signal phase
- ϕ_{B} is a phase bias

This MPF yields the basic information for antenna calibration and performance assessment. The MPF is nearly a straight line function over a large portion of the main beam. This is similar in shape to the phase-sensing

system described by Cohen and Steinmetz [3]. However, the Δ and Σ components in (3) are formed in software from baseband samples of the inphase and quadrature phase detected signals for both Σ and Δ.

A best approximation to (3) is obtained by using a linear least squares regression technique over the pre-specified fit interval. Typical results are shown in Figs. 8a and 8b. Figure 8a shows the actual measured MPF and the computed fit. The lower curve, 8b, shows how well the computed MPF fits the data by plotting the residual error vs. scan angle. It shows that errors considerably less than 0.008° are achieved.

The fact that the MPF can be modeled with a straight line over 60% of the sum beamwidth with residual errors on the order of 0.003° provides the basis to perform off-axis estimation as in (1). While beamsplitting ratios of 40:1 are readily achievable [4] in fixed beam antennas operating over small frequency bandwidths, this system is providing beamsplitting on the order of 100:1 for a scanned beam operating over relative wide frequency bandwidths.

The primary calibration parameter is the beam pointing error which is measured by determining the zero crossing of the fitted MPF. This yields the absolute beam position relative to the surveyed transmitter azimuth angle. The curves plotted in Fig. 8 are shown relative to the MPF zero crossing, but the pointing errors are absolute errors referred to the nominal beam position and the surveyed transmitter location.

The second calibration parameter is the slope of the MPF normalized by the cosine of the nominal beam position relative to array broadside. This normalization accounts for the $1/\cos\theta$ beamwidth broadening normally expected for a phased array scanned off broadside. The MPF slopes are always tabulated in the normalized form.

The previous section indicated a method of reducing the antenna sum and difference patterns into a monopulse function from which the critical calibration parameters (beam pointing error and monopulse slope) are obtained. Across the full field of view, the array has 961 such beam patterns and posi-

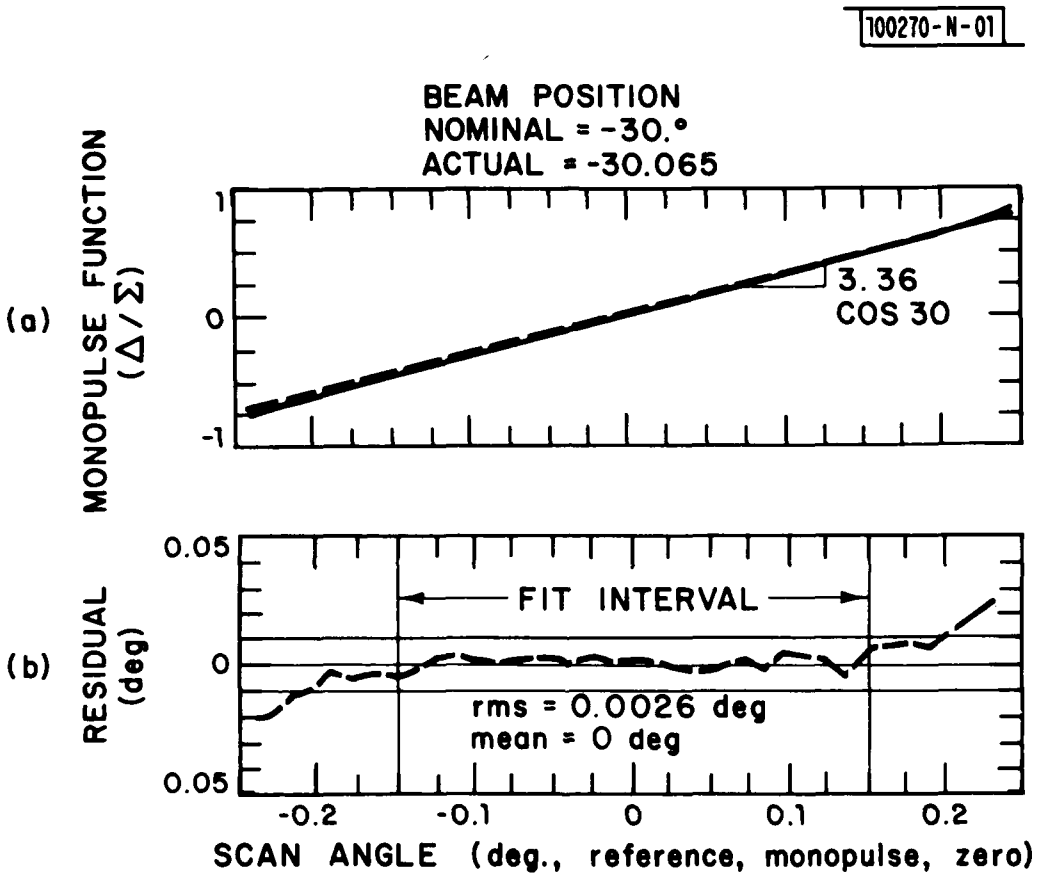

Fig. 8. Linear fit to monopulse function.

tions. The prime ojective of the measurement program is to summarize and assess these measurements.

Typically, a calibration run over the full ±30° field of view consisted of 61 beam position measurements taken with 1° spacing. Results are shown in Figs. 9 and 10 for the beam pointing error and the normalized monopulse slope respectively. Figure 9 indicates that each position has a beam pointing error of a few hundredths of a degree and this error is uncorrelated for beam positions separated by 1°. The normalized slope, in Fig. 10, shows a good position to position correlation and is virtually constant over the full field of view. This means that a single slope value will be sufficient for each frequency of operation.

Figures 11 and 12 show the beam pointing error and the normalized monopulse slope for each beam over a 3 degree interval with 1/16° spacing. Again it is seen that each position has a beam pointing error of a few hundredths of a degree and this error is uncorrelated for adjacent beam positions. As expected, the normalized monopulse slope shows excellent adjacent position correlation.

Figures 13 and 14 show the effect of frequency on the beam pointing error and monopulse slope. The frequencies shown on these two graphs are chosen to illustrate maximum effect. The 16.19 GHz is a frequency at which the antenna has been aligned (collimated) and 16.25 GHz is one half the distance between it and the next collimation frequency of 16.31 GHz. The beam programmer stores phase shifter calibration data in a look up table for four equally spaced frequencies. It uses the data for the nearest collimation frequency to determine the phase shifter values for a given operating frequency. Figure 13 shows that at the 16.25 GHz frequency the beam pointing error is uncorrelated from beam position to beam position. Moreover, as the frequency is varied, the pointing error is independent for each position.

In summary, the beam pointing errors are due to phase shifter random errors and quantization. The theoretical beam pointing error bound for a 200 element 3 bit phase shifter array is 0.012° assuming a 21° rms phase error. This compares well against our measured data.

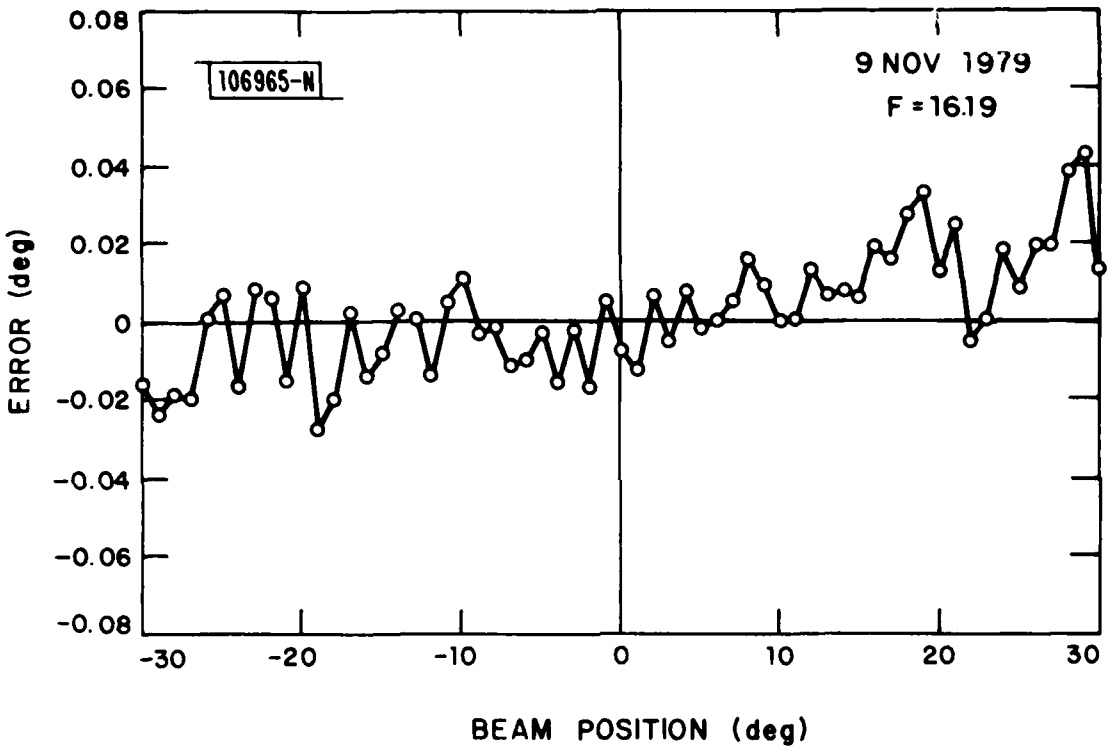

Fig. 9. Beampointing error for beam positions at 1° intervals.

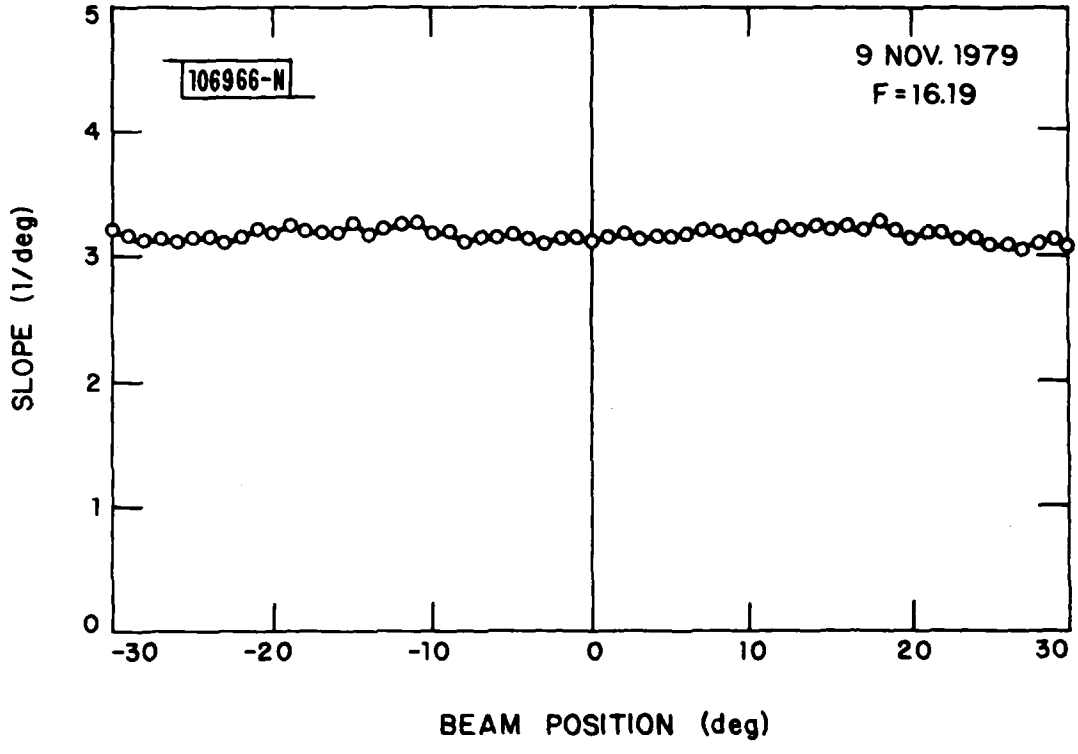

Fig. 10. Beampointing slope for beam positions at 1° intervals.

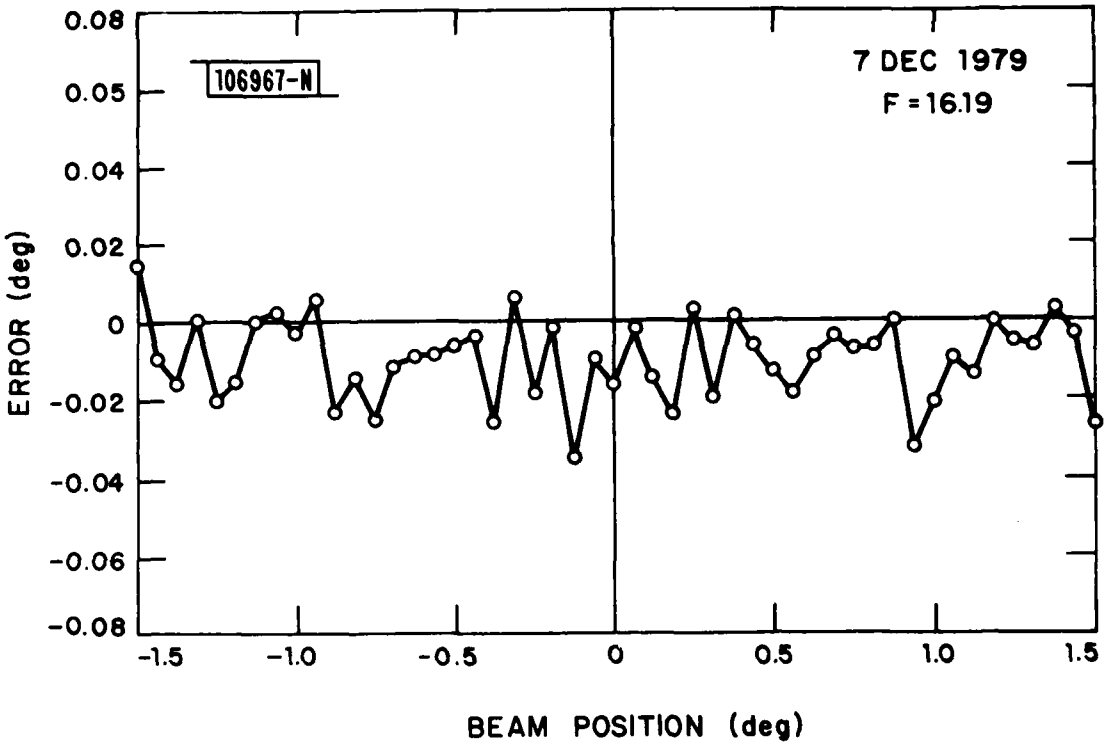

Fig. 11. Beampointing error for contiguous beam positions.

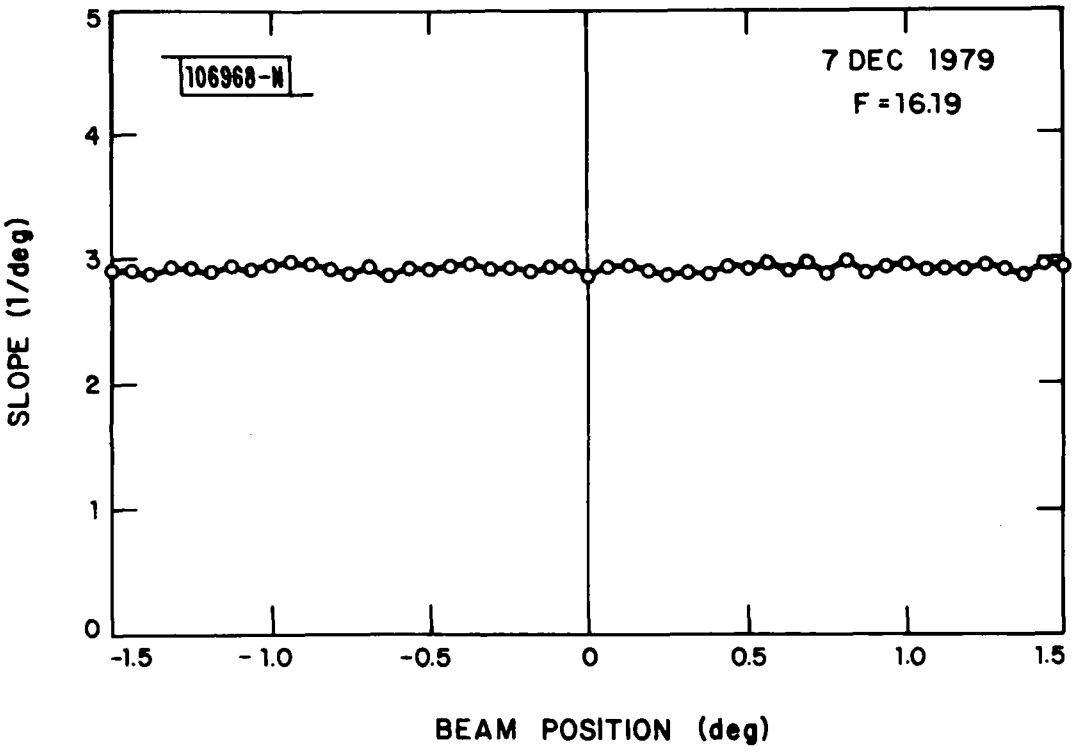

Fig. 12. Beampointing slope for contiguous beam positions.

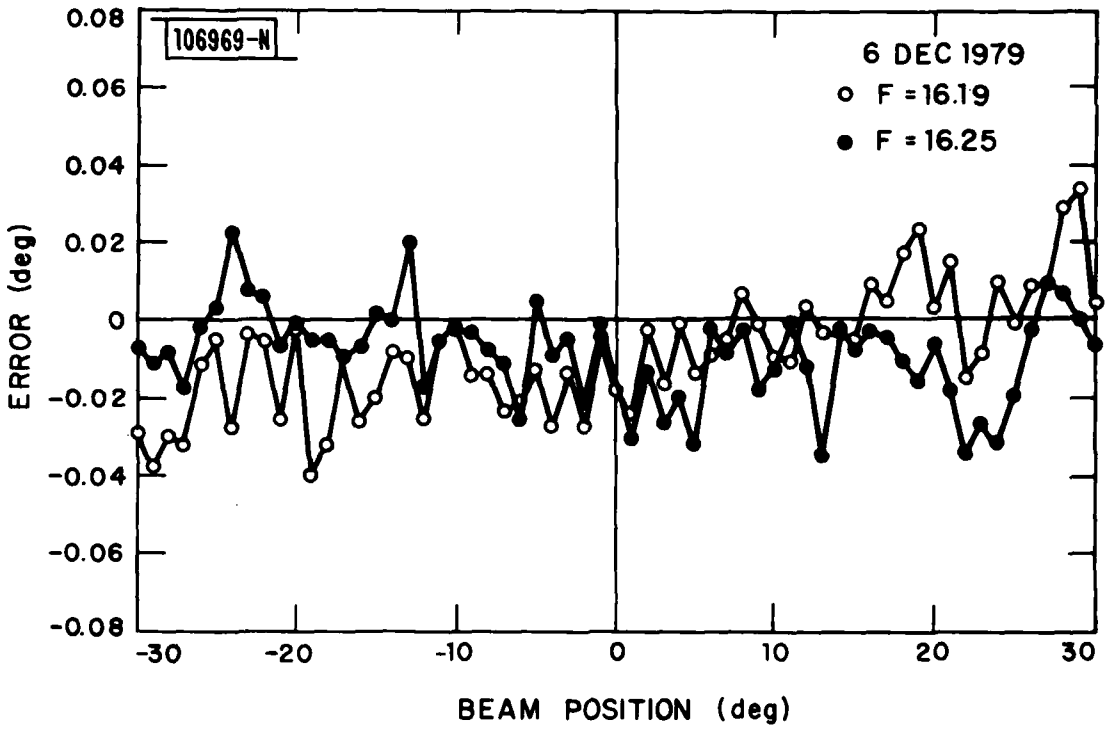

Fig. 13. Beampointing error frequency comparison.

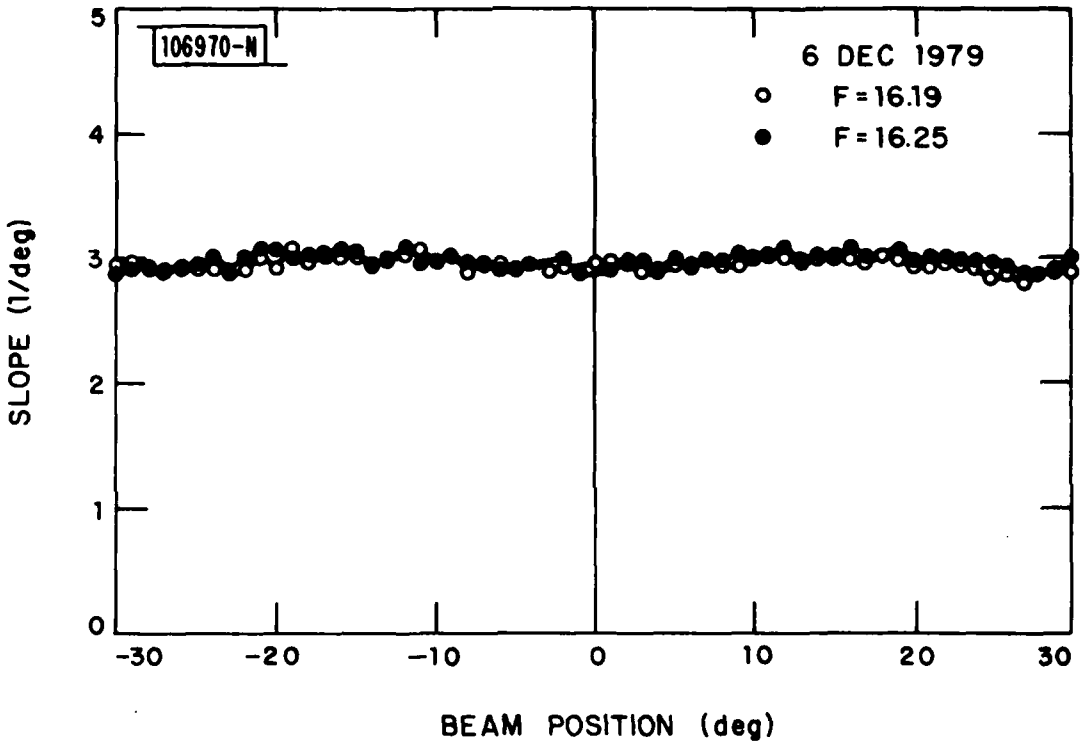

Fig. 14. Beampointing slope frequency comparison.

Although the beampointing error is frequently called non-removable and non-predictable for an ensemble of arrays, this error is invariant over time for a single antenna. Once the beam pointing error is measured for each beam position-frequency combination, it can be stored and used as a calibration correction.

VI. LONG TERM ANTENNA PERFORMANCE

The antenna array was operated daily over a five week period in the fall of 1979 to assess its long term performance and in particular the beam pointing stability. The metric cross range performance and calibration concept for a PSGA application depends on the beam pointing time stability and not on its absolute position. Thus, in spite of the fact that the beam pointing error is on the order of a few hundredths of a degree and uncorrelated from position to position, the pointing accuracy of 0.008° can be achieved if the PSGA exhibits the required time stability in a tactical operating environment. Thus, the net performance is based on the position uncertainty during the intracalibration period.

The PSGA stability results are summarized in the beampointing error histogram shown in Fig. 15. This is a composite of data taken at seven beam positions (i.e., -30, -20, -10, 0, 10, 20, and 30 degrees) equally spaced at 10° intervals across the array field of view. Each graph is plotted relative to its mean, and these are added to represent the entire antenna. The standard deviation for the antenna is found to be 0.0057 degrees and this is also shown on the graph. The corresponding 200 km cross range errors are shown on the top of the graph and it is noted that the pointing error standard deviation corresponds to a cross range error of 19.9m at 200 km.

The companion histogram for the slope is shown in Fig. 16. The events are relative to a mean slope of 3.12 degrees^{-1} and show a standard deviation of 0.093 from this mean. When a slope error is present, the residual error will increase across the monopulse function. This scale is shown on the bottom of this histogram with a translation to cross range error shown at the top of the graph. The standard deviation in the monopulse function slope has a corresponding cross range error of 9m at 200 km.

The results of this five week evaluation indicate the composite PSGA antenna RMS pointing error is .0063 degrees which is the RSS of the zero crossing and monopulse slope errors. This long term measured performance exceeds our design goal of 0 .008 degrees. Moreover as a result of the know-

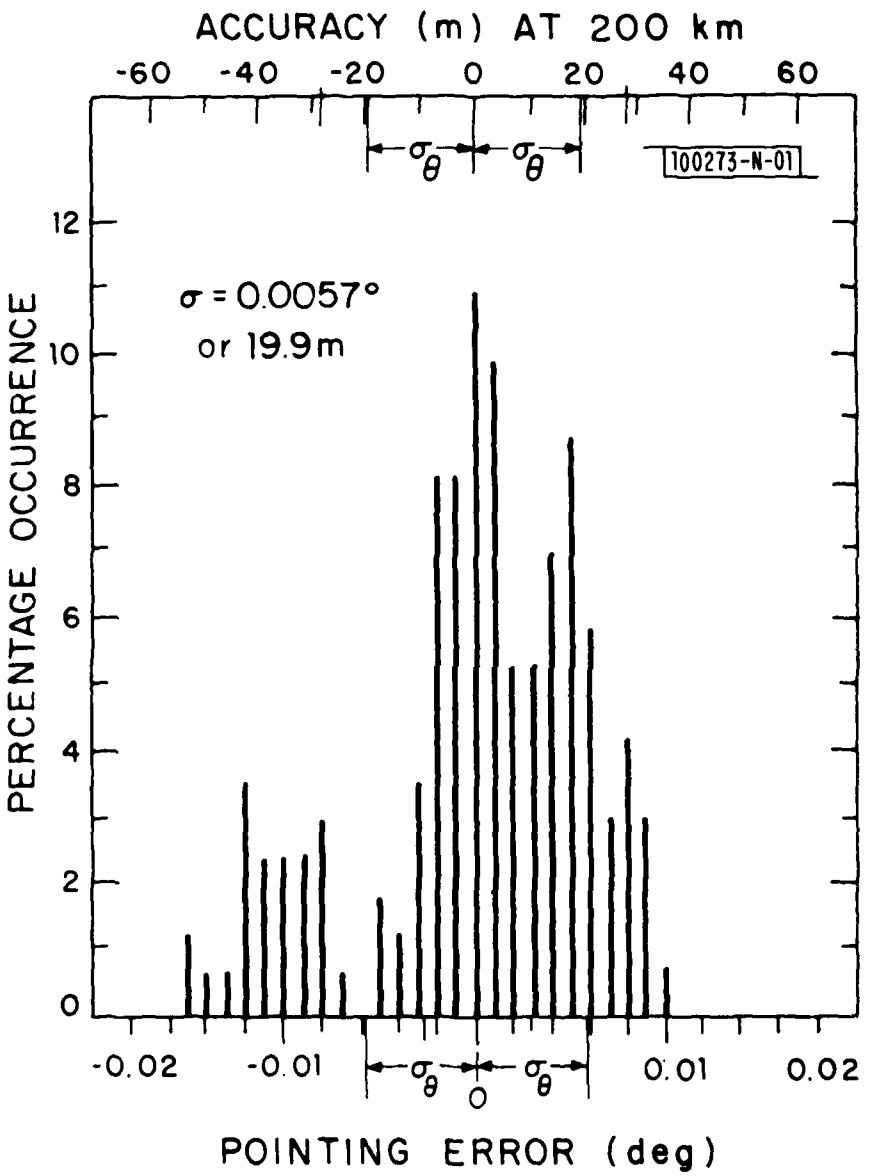

Fig. 15. Measured monopulse pointing error histogram.

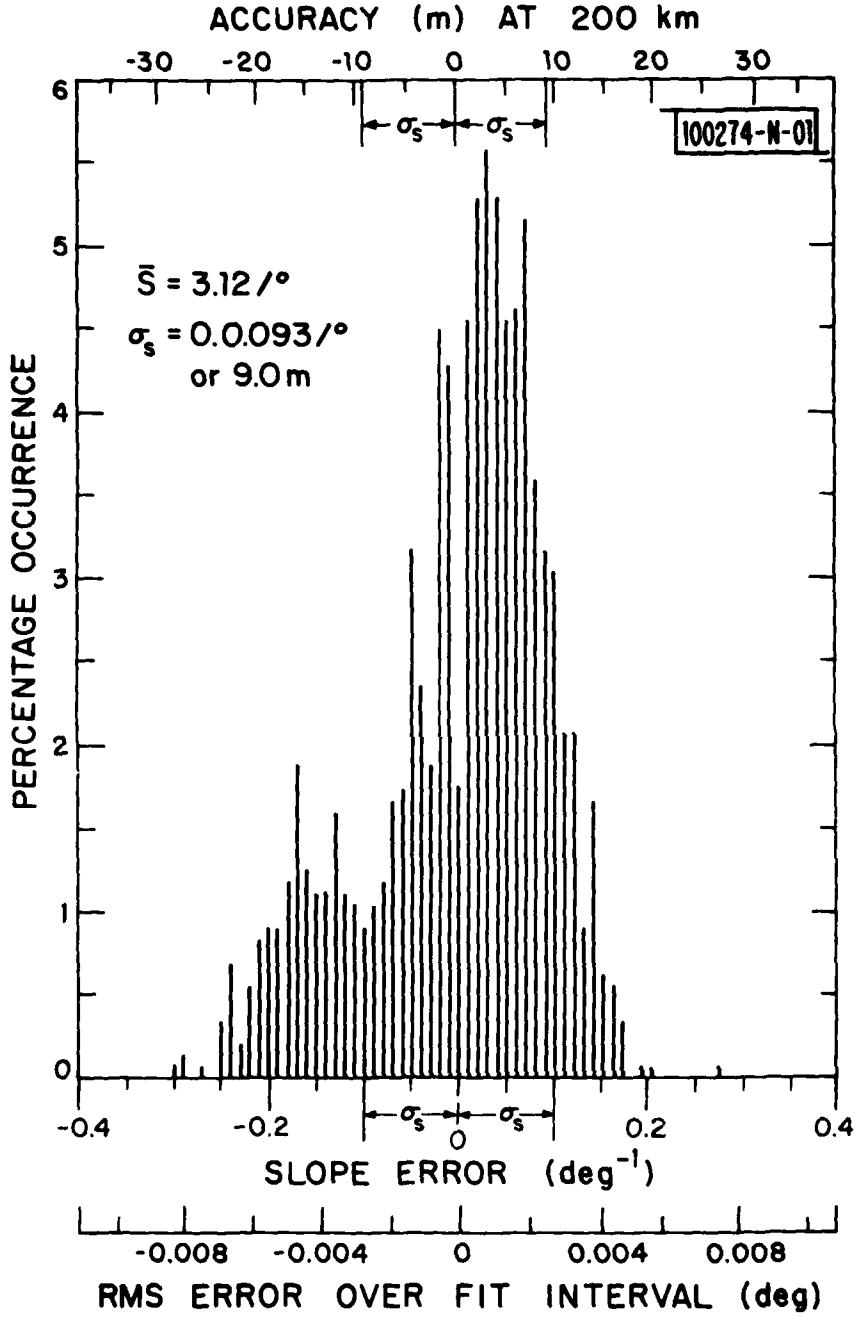

Fig. 16. Monopulse slope histogram.

ledge gained during this test, temperature compensation terms can be incorporated into the calibration model which can further reduce the residual error.

Prior to discussing the calibration model for the antenna, one should understand the typical and nontypical behavior of the pointing error as measured over the five week evaluation. Figures 17 and 18 show some representative results using 61 beam positions spaced at 1° intervals across the array field of view. The measured results are referenced to a set of data taken 4 hours earlier. The RMS change in the error is 0.0008 degrees.

Figures 19 and 20 show measured results on 4 different days over a 1 week period. The data are referenced to the Oct. 30 measurements. The Oct. 31, Nov. 1, and Nov. 2 data have an 0.0008, 0.0016, 0.0034 degree RMS error. The Nov. 2 data which has the largest error was probably caused by an array temperature change. As will be shown in a later section, these errors can be reduced by using a temperature sensitive calibration model.

Figure 21 shows representative results measured over a three week interval. The measured results are referenced to a set of data taken on 15 Nov. 1979. With respect to this reference, the four curves show both positive and negative shifts and positive and negative tilts. The curve of 29 Oct. shows basically a positive shift while 19 Nov. shows a negative shift. The curves of 2 Nov. and 8 Nov. show negative and positive tilts respectively. Shift is due to phase changes in the phase shifters or receiver while tilt is due to uniform array expansion. Both effects are due to temperature variations on the array. A significant observation is that relative pointing errors are confined within ±0.006 degree limits fairly well over this relatively long observation period.

The data have now been presented to justify a proposed calibration model. As pointed out earlier, two components are needed for each (ith) position. For the slope, all that is needed, is Eqn. (4).

$$S_i = S(f) \cos \theta_i \qquad (4)$$

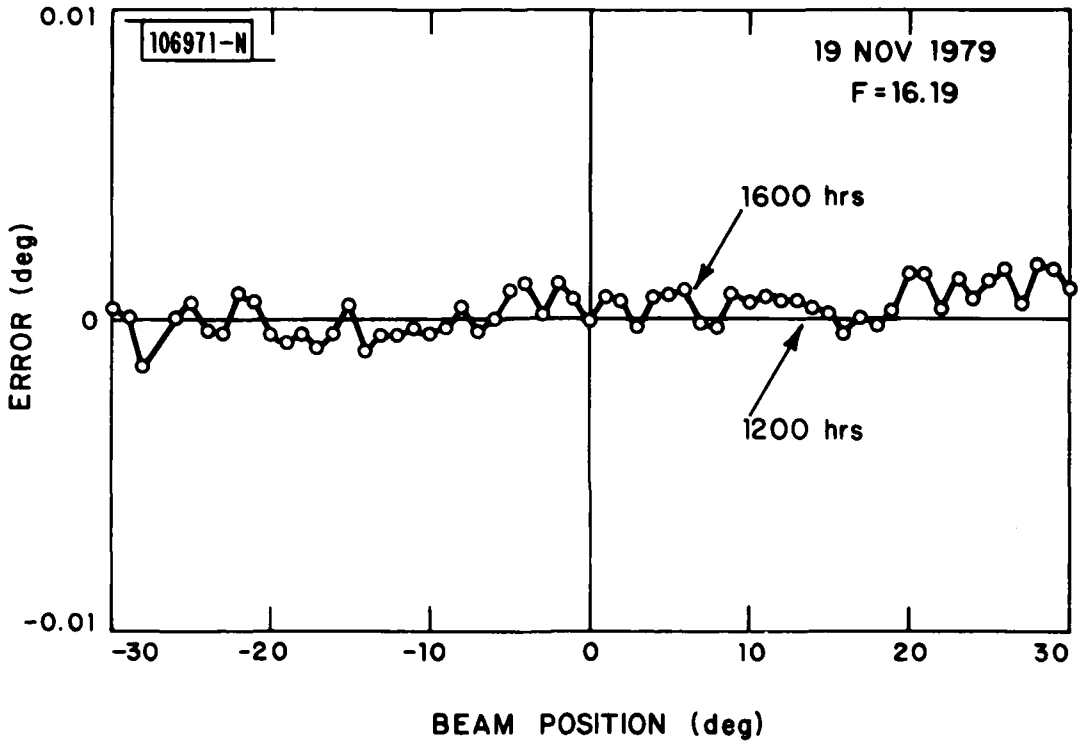

Fig. 17. Beampointing error comparison after four hours.

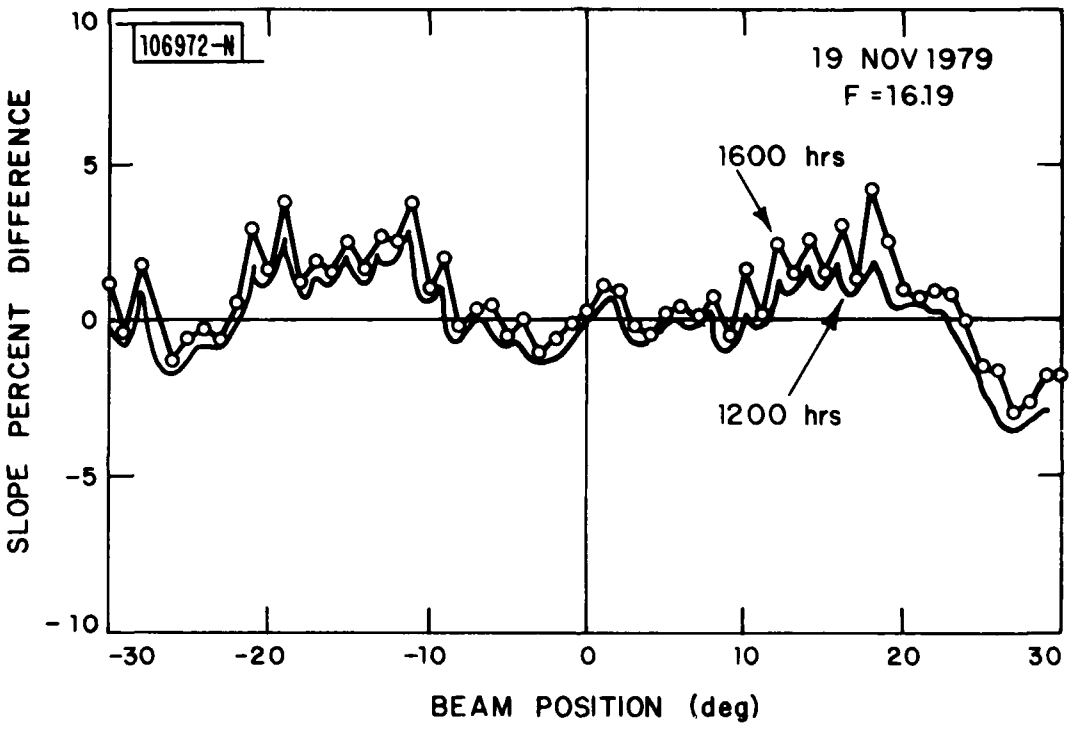

Fig. 18. Beampointing slope comparison after four hours.

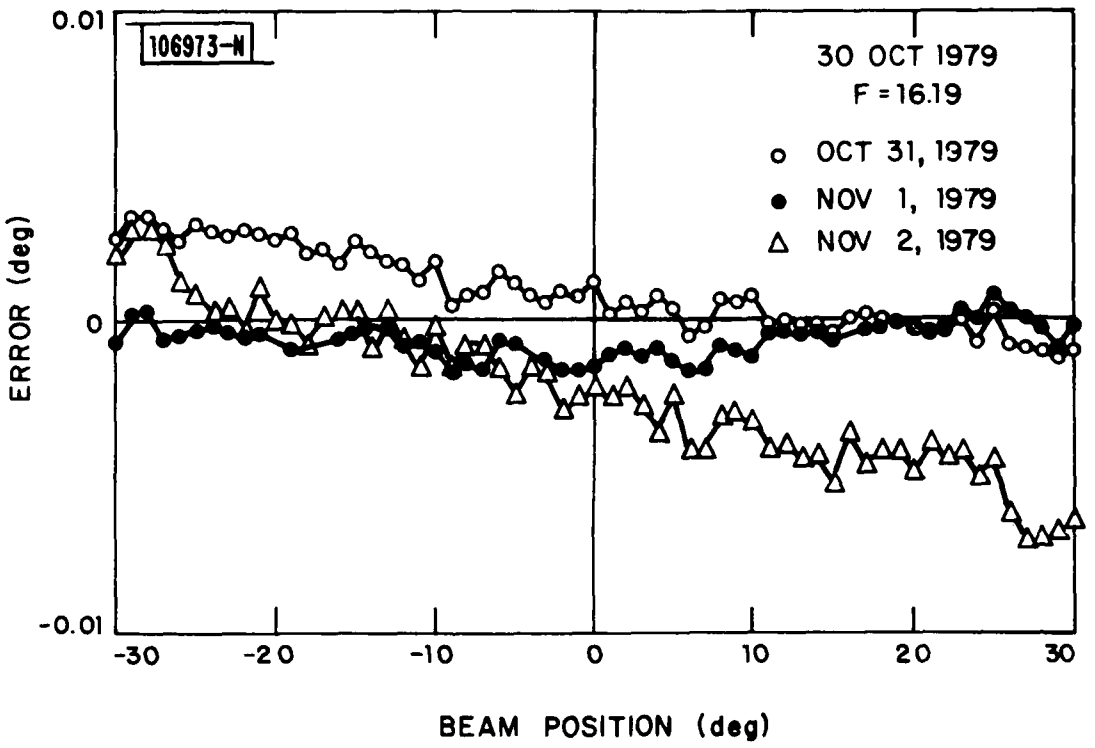

Fig. 19. Beampointing error comparison over one week.

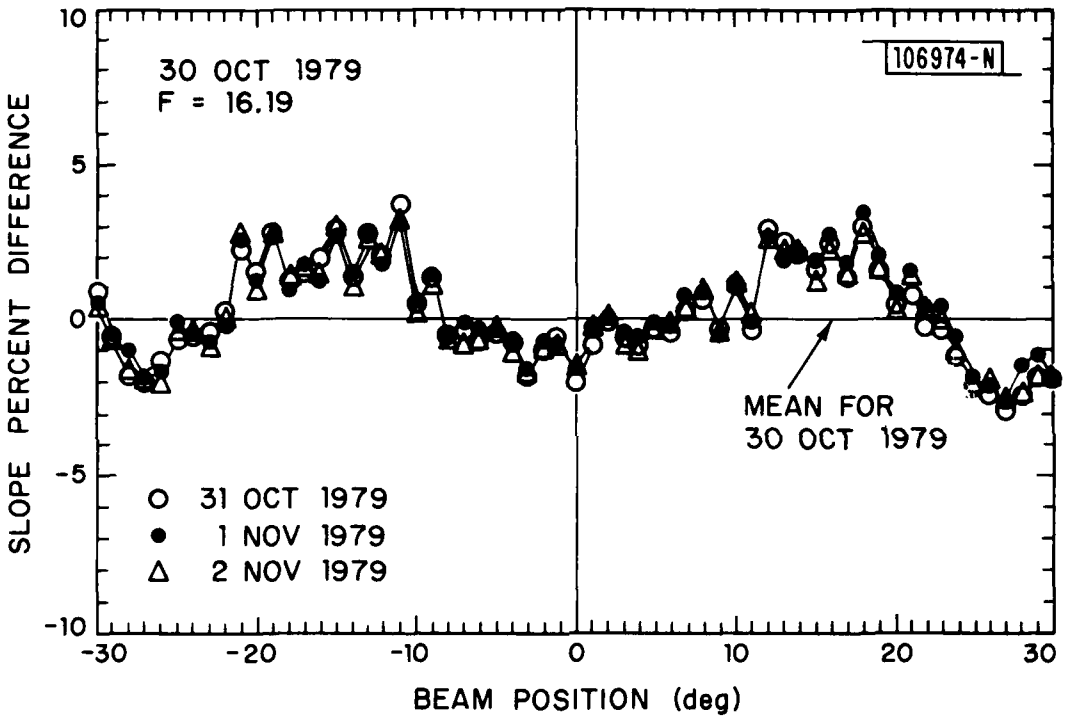

Fig. 20. Beampointing slope comparison over one week.

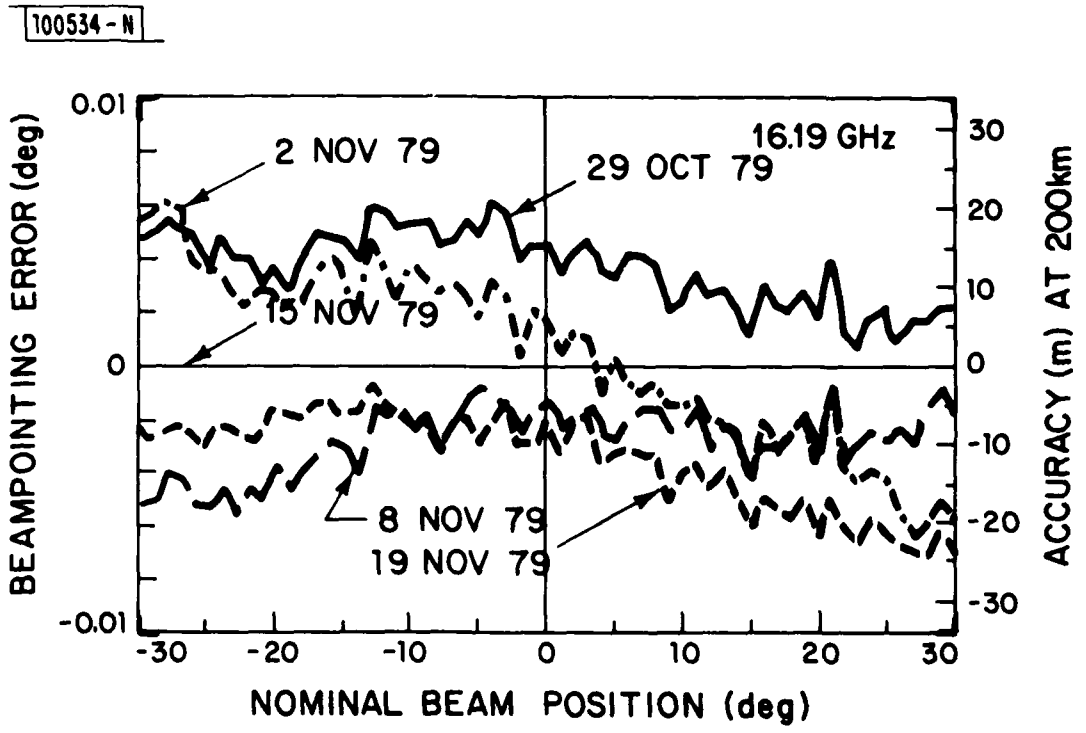

Fig. 21. Long term beampointing error.

where a normalized mean value is obtained for each frequency of operation. θ_i is the nominal beam position. For the estimated beam position, Eqn. (5) is sufficient.

$$\theta_{ei} = \theta_i + BPE_o(f) + LU\ (\theta_i, f) \tag{5}$$

Here there are broadside errors for each frequency of operation, in BPE_o, while off broadside positions are estimated relative to broadside in a look up table, LU. The equations are broken up this way to accommodate temperature effects which will be discussed later. It should be noted however that BPE_o affects a shift in the curve while LU can affect the tilt in the curve for off broadside performance.

Finally, the number of elements for this model is given in (6).

$$\text{No.} = (200 \text{ positions} + 1 \text{ slope}) \times 51 \text{ frequencies}$$

$$= 10251 \text{ elements} \tag{6}$$

The 200 positions are chosen to span the 60 degree field of view with the nominal fit interval of 0.3 degree per beam position. The linear behavior was sufficient to support this conclusion. The significance of this model is that the long term stability of the antenna provides a repeatable relative pointing error curve and so 199 elements for each frequency do not have to be recalibrated very often, if ever. This leaves one percent or 102 elements of the model that would need to be recalibrated for a mission, which is a substantial reduction over what was anticipated at the outset of this program.

VII. MODEL PERFORMANCE

The previous section has set forth a model for the antenna performance in Eqs. (4) and (5). In this section, the model will be evaluated by means of analytic and measured results. As was pointed out earlier, the performance for any operating frequency is typical for all operating frequencies. Thus, only a single operating frequency will be considered in the evaluation of the model performance.

Figure 22 illustrates the manner in which the model of Eqs. (4) and (5) may be applied to estimate the expected residual errors for a given beam position. The expected squared residual error over the full beam interval is given in Eqn. (7).

$$E_I(R_i^2) \approx \sigma_{\theta_m}^2 + (\theta_f \sigma_{S_m}/\sqrt{3}/S_i)^2 \qquad (7)$$

Eqn. (7) was obtained by using uniform probability distributions, for both S_m and θ_m, and has been simplified using the fact that θ_f^2 is much greater than $\sigma_{\theta_m}^2$. The measured statistics (shown earlier in the histograms) can be used to evaluate the expected errors in the antenna system. When these data are substituted into (7), the results in Table 3 are found at broadside ($\theta_i = 0°$) and edge of the scan ($\theta_i = \pm 30°$), respectively. The results show that pointing error dominates the performance with a deviation of 0.0057° out of the expected performance of 0.0064° at the edge of the antenna field of view. The estimated residual error of 0.0063° is well below the goal of 0.0080° stated at the beginning of the report.

The above analysis of expected behavior is based on data taken over a five-week period spanning 29 October 1979 to 7 December 1979. In order to confirm the predicted behavior of the model, random tests were taken over a seven-week period spanning 17 March 1980 to 30 April 1980. The temperature of the antenna was not controlled for this run and was allowed to float with ambient temperature which ranged from 9°C to 33°C over this time span. The results of these tests are shown in Fig. 23.

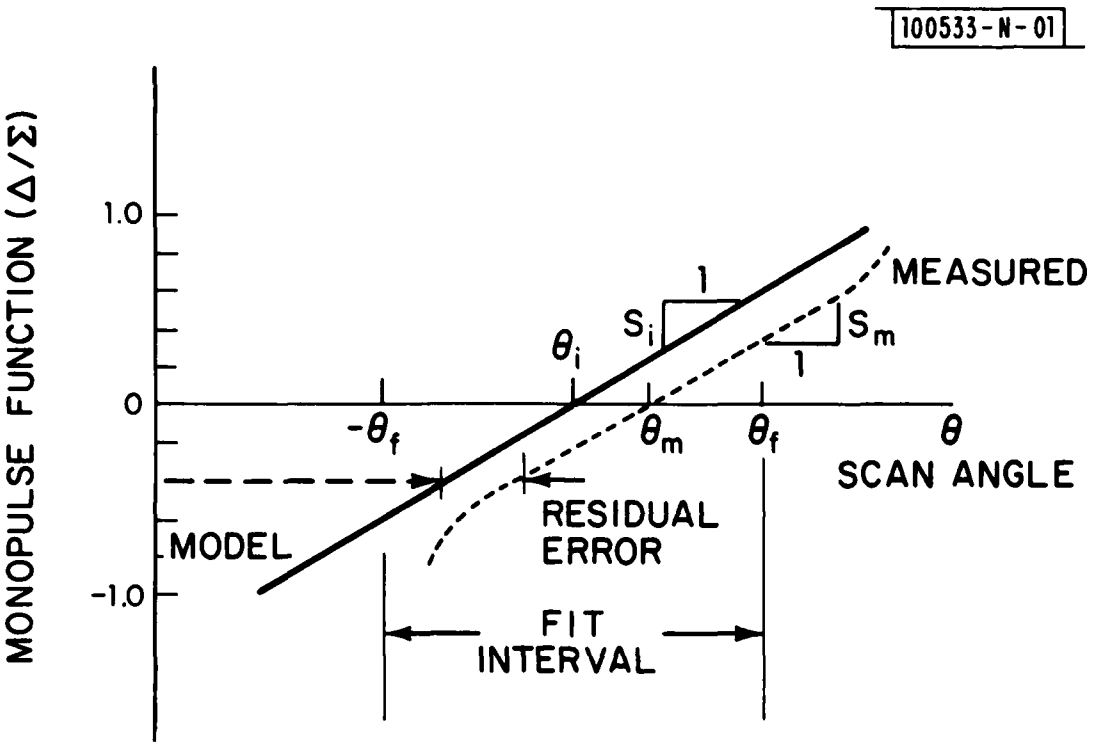

Fig. 22. Performance of monopulse model.

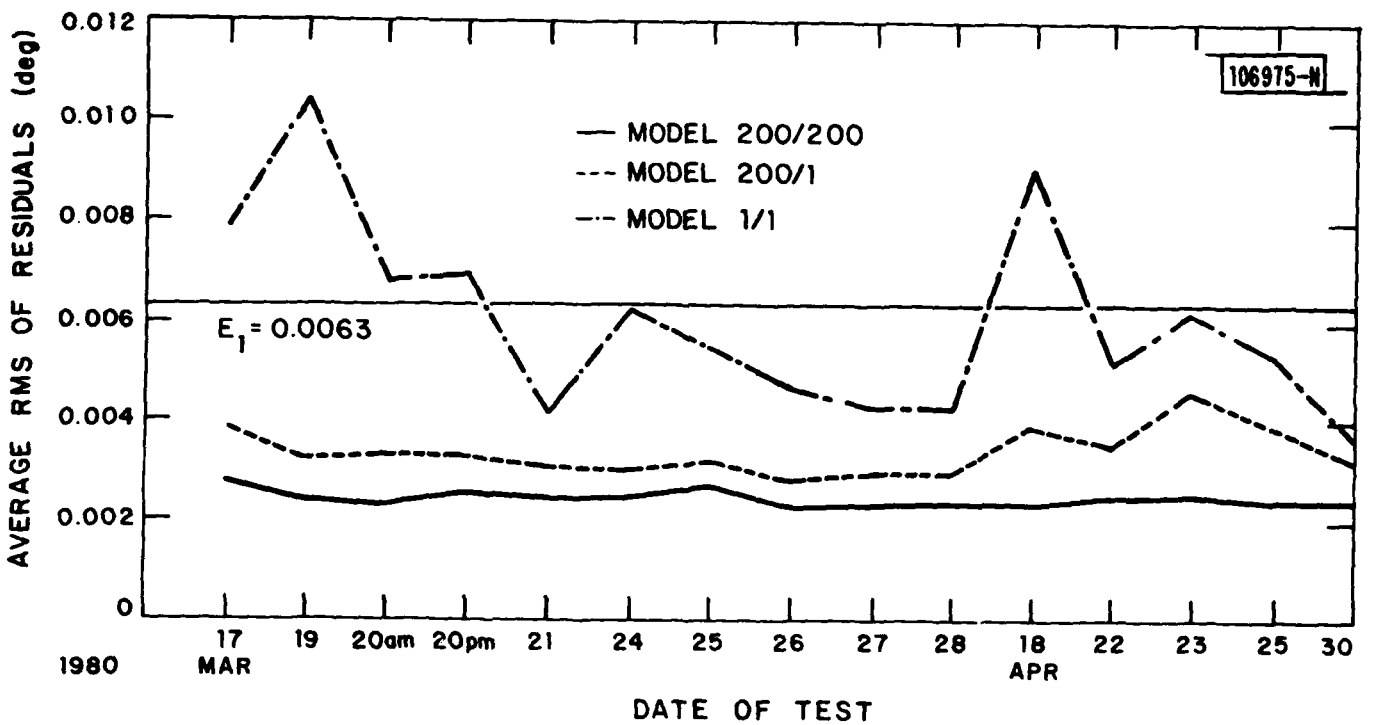

Fig. 23. Comparison of calibration model performance.

TABLE 3

EXPECTED PEFORMANCE

θ_i	$\sqrt{E_1}$
0°.	0063°
±30°.	0064°

$\theta_f = 0.15^\circ$, $\sigma_{\theta_m} = 0.0057^\circ$, $S(f) = 3.12\ \text{deg}^{-1}$, $\sigma_{s_m} = 0.093\ \text{deg}^{-1}$.

The results represent the average rms residual error across the full interval for each of 61 beams spaced 1° apart across the full ±30° field of view of the antenna. The three curves represent results obtainable with different levels of analysis. The first curve represents the performance obtainable from a best fit straight line model and uses each beam position and slope obtained for each day. The second curve represents the performance obtainable using best fit beam positions for each day with the slope determined from a single value as in Eq. (4). The result shows a loss of about 0.001° in accuracy over that of the first curve. Finally, the third curve represents the use of a look-up table to estimate each beam position and a single slope constant for each frequency. This analysis uses both Eqs. (4) and (5) and represents the proposed model for the antenna.

The results are plotted and can be compared to the estimated rms accuracy of 0.0063° as shown on the curve. Good statistical behavior is demonstrated around the expected error derived at the beginning of this discussion. Run No. 6 (Mar 24) is arbitrarily used for generating the look-up table and the slope constant for curves 2 and 3. The results are not significantly affected if a Nov. look-up table is used for LU in Eq. (5). The major conclusion is that the antenna possesses remarkably good long term stability and that the results are repeatable in a direct and simple fashion.

VIII. TEMPERATURE COMPENSATION

It was mentioned previously that temperature has a strong effect upon the angular accuracy of the antenna. Typically, a 4°C change in array temperature can cause a 0.01° pointing error. The runs taken in March 1980 allowed preliminary results to be obtained to provide temperature coefficients for this behavior. AT 16.190 GHz, Eqs. (4) and (5) are modified as in Eqs. (8) and (9).

$$S_i' = (S(f) - 0.0024\ \Delta T)\ \cos\theta_i \tag{8}$$

$$\theta_{ei}' = \theta_i + (BPE_o(f) + 0.00033\ \Delta T) + (LU(\theta_i, f) - 20\theta_i\ \Delta T \cdot 10^{-6}) \tag{9}$$

ΔT is measured relative to the calibration temperature of LU (18.6°C in this case). It is seen that a positive ΔT increment decreases the slope, offsets the look-up curve, and provides tilt vs. position, θ_i.

Figure 24 illustrates the use of Eqs. (8) and (9) to provide temperature compensation. These are both the proposed model and show what can be achieved with a single look-up table and calibration constants over a seven week period. Based on the average of maximum and minimum values for each curve, it is seen that temperature compensation improves uncompensated performance by nearly 0.002°. This is a useful improvement when compared to the expected performance of 0.0063°. Generally, it appears that the use of temperature compensation can produce results between that of the second analysis discussed in Section VII and the predicted error, E_1.

This is an important result when the practical application of the antenna is considered. Large temperature variations will be encountered for a platform operating at high elevations, and temperature compensation will have to be used to reduce errors in the system. The results of this analysis are encouraging for this important application.

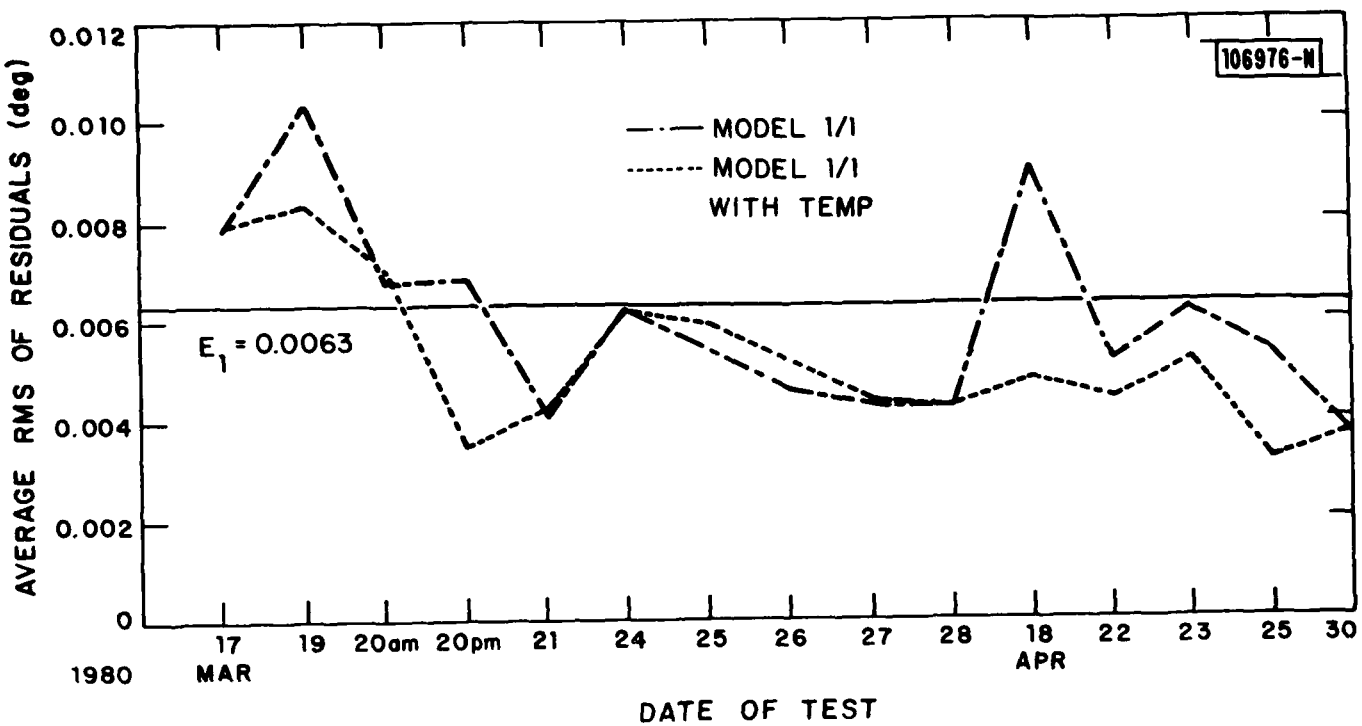

Fig. 24. Calibration model performance comparison with temperature compensation.

IX. CONCLUSIONS

The PSGA performance evaluation has demonstrated that it can support the beampointing accuracy requirements for single station guidance using a simple calibration model. Moreover, the antenna stability was found to be such that recalibrations are rarely required.

The angular accuracy required to place the weapon platform within a 50 m cross range tolerance from a 200 km standoff is 0.0143 degrees. The PSGA must provide accuracies of less than 0.008 degrees to make this concept viable. The test results showed the proposed model provides an average rms error on the order of 0.007 degrees without temperature compensation and 0.006 degrees with compensation. It is clear that whether temperature compensation is used or not, the required angular accuracy is obtained for ground applications.

The above test results were obtained using a straight line model. This is a much simpler model than that expected at the onset of the program. At each operating frequency the model uses a single value for monopulse slope and a broadside pointing error. Beam positions off broadside are estimated from a look up table depicting relative beampointing errors. This model has a total of 201 calibration parameters at each operating frequency. The prime advantage of this model is that only 2 parameters, the broadside pointing offset and monopulse slope need to be updated whenever recalibration is required.

The stability of the antenna permitted the development of this model. The performance evaluation showed the required beampointing performance for single station standoff guidance was achieved for time periods measured in weeks without recalibration.

ACKNOWLEDGMENTS

This work represents the collective results of several people involved with both the hardware and software effort. Those making significant contributions to the project are as follows. Gary Jordan for developing the edit and analysis software, Carol Catalano for developing the data collection and system control software, Ken Fowler for operations control, Bob Pritchard and Emil Eastburn for the design, construction and debugging of the guidance microcomputer, Bob Parr for design in the A/D and downconverter system, Andy Vierstra for the design of the dual channel RF receiver and acceptance testing of the PSGA, Jim Bertram for the layout and construction of the RF receiver, Joe Kulpa for construction and maintenance of the pedestal and encoder systems, Paul McGarry for the error detector circuitry in the beam programmer, Roger Burgess for invaluable digital system consultation, and importantly the secretaries, Diane Young and Nancy Campbell, who made many viewgraphs and typed many versions of this work. The work required to achieve the results obtained had to be of high quality and is recognized and appreciated by both authors.

A special acknowledgment is due to Dr. Harry Lee for initiation of the concepts behind single station guidance and for his organization of the program. He brought the problem and the team together and his contributions have assured its ultimate success.

REFERENCES

1. C.J. Miller, "Minimizing the Effects of Phase Quantization Errors in a Electronically Scanned Array," Proc. 1964 Symp. Elect. Scanned Array Tech. & Appl., Griffiss Air Force Base, Rome, NY, RADC-TDR-64-225, Vol. 1, pp. 17-38.

2. R.H. Sahmel and R. Manasse, "Spatial Statistics of Instrument-Limited Angular Measurement Errors in Phased Array Radars," IEEE Trans. Antennas Propag. AP-21, 524 (1973).

3. W. Cohen and C.M. Steinmetz, "Ampltiude- and Phase-Sensing Monopulse System Parameters, Part 2," Microwave J. 2, 33 (1959).

4. K. Karp and M.L. Wood, "DABS Monopulse Summary," Project Report ATC-72, Lincoln Laboratory, M.I.T. (4 February 1977), DDC AD-A038157/4.

UNCLASSIFIED

SECURITY CLASSIFICATION OF THIS PAGE (When Data Entered)

REPORT DOCUMENTATION PAGE

READ INSTRUCTIONS BEFORE COMPLETING FORM

1. REPORT NUMBER: ESD-TR-81-6	2. GOVT ACCESSION NO.: AD-A103063
3. RECIPIENT'S CATALOG NUMBER:	
4. TITLE (and Subtitle): Precision Standoff Guidance Antenna Accuracy Evaluation	5. TYPE OF REPORT & PERIOD COVERED: Technical Report
	6. PERFORMING ORG. REPORT NUMBER: Technical Report 543
7. AUTHOR(s): Fred H. Irons and Melvin M. Landesberg	8. CONTRACT OR GRANT NUMBER(s): F19628-80-C-0002
9. PERFORMING ORGANIZATION NAME AND ADDRESS: Lincoln Laboratory, M.I.T. P.O. Box 73 Lexington, MA 02173	10. PROGRAM ELEMENT, PROJECT, TASK AREA & WORK UNIT NUMBERS: Program Element No. 63750F Project No. 2335
11. CONTROLLING OFFICE NAME AND ADDRESS: Air Force Systems Command, USAF Andrews AFB Washington, DC 20331	12. REPORT DATE: 18 February 1981 13. NUMBER OF PAGES: 54
14. MONITORING AGENCY NAME & ADDRESS (if different from Controlling Office): Electronic Systems Division Hanscom AFB Bedford, MA 01731	15. SECURITY CLASS. (of this report): Unclassified 15a. DECLASSIFICATION DOWNGRADING SCHEDULE

16. DISTRIBUTION STATEMENT (of this Report)

Approved for public release; distribution unlimited.

17. DISTRIBUTION STATEMENT (of the abstract entered in Block 20, if different from Report)

18. SUPPLEMENTARY NOTES

None

19. KEY WORDS (Continue on reverse side if necessary and identify by block number)

phased array
monopulse azimuth estimation
beam pointing calibration
beam splitting high ratio
beam splitting wide bandwidth

20. ABSTRACT (Continue on reverse side if necessary and identify by block number)

This report presents a summary of work done to determine the inherent angular accuracy achievable with the guidance and control precision standoff guidance antenna. The antenna is a critical element in the anti-jam single station guidance program since its characteristics can limit the intrinsic location guidance accuracy. It was important to determine the extent to which high ratio beamsplitting results could be achieved repeatedly and what issues were involved with calibrating the antenna.

The antenna accuracy has been found to be on the order of 0.006° through the use of a straightforward lookup table concept. This corresponds to a cross range error of 21 m at a range of 200 km. This figure includes both pointing errors and off-axis estimation errors.

It was found that the antenna off-boresight calibration is adequately represented by a straight line for each position plus a lookup table for pointing errors relative to broadside. In the event recalibration is required, it was found that only 1% of the model would need to be corrected.

DD FORM 1 JAN 73 1473 EDITION OF 1 NOV 65 IS OBSOLETE

UNCLASSIFIED

SECURITY CLASSIFICATION OF THIS PAGE (When Data Entered)

20765

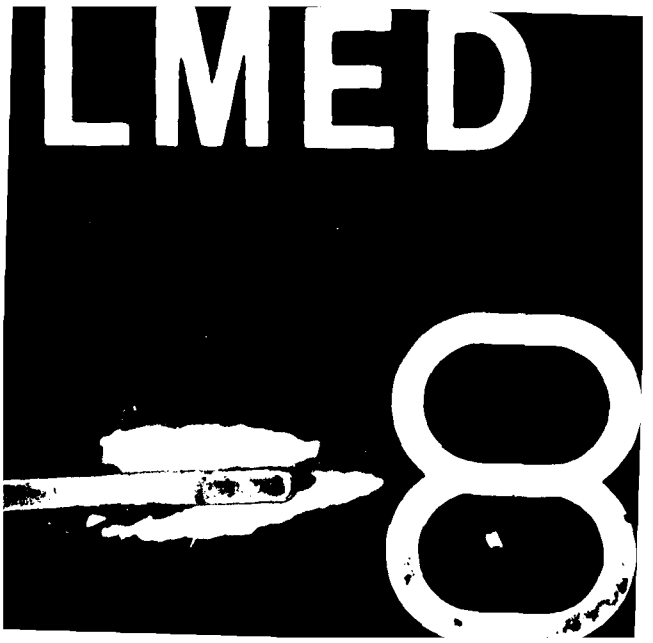
LMED
8